

Photodissociation and photoisomerization dynamics of CH₂=CHCHO in solution

Weiqliang Wu, Chunfan Yang, Hongmei Zhao, Kunhui Liu, and Hongmei Su^{a)}

State Key Laboratory of Molecular Reaction Dynamics, Beijing National Laboratory for Molecular Sciences (BNLMS), Institute of Chemistry, Chinese Academy of Sciences, Beijing 100190, China

(Received 2 December 2009; accepted 9 February 2010; published online 30 March 2010)

By means of time-resolved Fourier transform infrared absorption spectroscopy, we have investigated the 193 nm photodissociation and photoisomerization dynamics of the prototype molecule of α,β -enones, acrolein (CH₂=CHCHO) in CH₃CN solution. The primary photolysis channels and absolute branching ratios are determined. The most probable reaction mechanisms are clarified by control experiments monitoring the product yields varied with the triplet quencher addition. The predominant channel is the 1,3-H migration yielding the rearrangement product CH₃CH=C=O with a branching ratio of 0.78 and the less important channel is the α cleavage of C—H bond yielding radical fragments CH₂=CHCO+H with a branching ratio of only 0.12. The 1,3-H migration is strongly suggested to correlate with the triplet ³($\pi\pi^*$) state rather than the ground S₀ state and the α cleavage of C—H bond is more likely to proceed in the singlet S₁ ¹($n\pi^*$) state. From the solution experiments we have not only acquired clues clarifying the previous controversial mechanisms, but also explored different photochemistry in solution. Compared to the gas phase photolysis which is dominated by photodissociation channels, the most important channel in solution is the photoisomerization of 1,3-H migration. The reason leading to the different photochemistry in solution is further ascribed to the solvent cage effect. © 2010 American Institute of Physics. [doi:10.1063/1.3352421]

I. INTRODUCTION

The rich photochemistry of the enone functional group —C=C—C=O is still yielding new reliable reactions widely used as key synthetic methodologies in various fields.^{1–7} As the simplest α,β -enones, acrolein (CH₂=CHCHO) serves to be an ideal molecule for studying the interesting photochemistry of this class of important molecules. On account of the interacting ethylenic and carbonyl chromophores, the photochemistry of enones is extremely varied. In addition to the photochemistry of the C=O chromophore (α -cleavage, H-abstraction, and the Paterno-Buchi reaction^{8,9}) and the C=C chromophore [e.g., (² π +² π) cycloadditions], α,β -enones undergo a variety of photochemical rearrangements of the C=C—C=O moiety.^{10,11}

CH₂=CHCHO has two conformers: *s-trans* and *s-cis*, with *s-trans* being the more stable one. (See Scheme 1.) Alves *et al.*¹² showed that about 96% of the ground-state acrolein is present as the *s-trans* conformer at 293 K with slight decreasing probability at higher temperature. CH₂=CHCHO has been subject to many previous spectroscopic investigations. Six absorption bands were observed by Walsh *et al.*¹³ at different wavelengths. The weak band starting at 412 nm and the strong one at 387 nm were assigned to S₀-T₁ and S₀-S₁ state transitions, respectively. Beck *et al.*¹⁴ suggested the existence of fast internal conversion (IC) or intersystem crossing (ISC) from S₁ to S₀ and T₁ state due to the low yield of fluorescence. At shorter wavelength, a strong

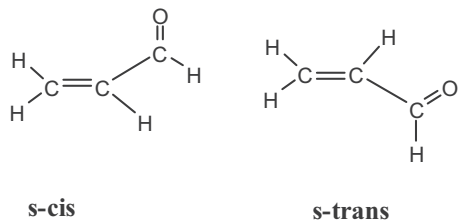
diffuse band centered at 193.5 nm has been also observed. On the basis of *ab initio* self-consistent-field (SCF) calculations this band was attributed to a $\pi \rightarrow \pi^*$ transition.^{15–17}

The gas phase photolysis of CH₂=CHCHO has been extensively investigated. Three primary channels, the HCO, H, and CO loss channels, have been observed in the near UV to UV range



The channels (1) and (2) involve separately the α cleavage of the C—C or C—H bond and the channel (3) corresponds to a molecular decarbonylation process. Shinohara and Nishi¹⁸ observed CH₂CH and HCO as the only primary products for the photofragmentation of acrolein in supersonic molecular beam at 193 nm. They suggested that the C—C bond fission to HCO+CH₂=CH occurs in the S₁ state (¹ $n\pi^*$) after IC from the initially excited S₂ state (¹ $\pi\pi^*$). For the H loss channel (2), Butler *et al.*¹⁹ employed H-atom high-n Rydberg tagging time-of-flight mass spectroscopy to measure the H-atom velocity distribution and suggested that C—H bond fission process in CH₂=CHCHO at 193 nm involves the fission of the aldehydic bond. Their observation of a translational energy distribution peaked away from 0 is consistent with a significant barrier to the reverse reaction which indicates that the C—H bond fission channel probably proceeds in the (¹ $n\pi^*$) state or (³ $n\pi^*$) state rather than the ground S₀

^{a)}Author to whom correspondence should be addressed. Electronic mail: hongmei@iccas.ac.cn.



SCHEME 1. Structure of acrolein.

state since the dissociation in the excited states involves a certain barrier in the exit channel. For the CO release channel (3), Lin *et al.*^{20,21} performed CO laser resonance absorption measurements for the photodissociation of two isomers of methylketene (CH_3CHCO) and acrolein (CH_2CHCHO) at 193 nm. The appearance times and the vibrational energy content of the CO formed were similar in the two systems, indicating that in the case of acrolein, isomerization to methylketene takes place prior to the dissociation process: $\text{CH}_2=\text{CHCHO} \rightarrow \text{CH}_3\text{CH}=\text{CO} \rightarrow \text{CH}_3\text{CH}+\text{CO} \rightarrow \text{CH}_2\text{CH}_2+\text{CO}$. Such a process was proposed to occur in the highly, vibrationally excited ground S_0 state. With a molecular beam time-of-flight apparatus, Huber and co-workers²² have identified the above three photolysis channels (1)–(3) and speculated that the dissociation processes of acrolein at 193 nm occurred in the lower electronic states after IC or ISC processes from initial higher state. Hot photofragments in three channels underwent secondary dissociation processes of $\text{HCO} \rightarrow \text{H}+\text{CO}$, $\text{C}_2\text{H}_3 \rightarrow \text{C}_2\text{H}_2+\text{H}$, $\text{CH}_2=\text{CHCO} \rightarrow \text{C}_2\text{H}_3+\text{CO}$.

Apart from the experimental studies, a few theoretical studies on ground and excited state surfaces of $\text{CH}_2=\text{CHCHO}$ are also available.^{15,23–26} In a recent work, Fang and co-workers²⁷ have mapped potential energy surfaces of the S_0 , T_1 $^3(\pi\pi^*)$, T_2 $^3(n\pi^*)$, and S_1 $^1(n\pi^*)$ states of $\text{CH}_2=\text{CHCHO}$ by complete active space self-consistent field (CASSCF) method. The most probable mechanism leading to different products was proposed on the basis of the obtained potential energy profiles and their crossing points. Acrolein excited to the $^1(\pi\pi^*)$ state first relaxes to the $^1(n\pi^*)$ state. From this state, acrolein can decompose into the products via three different routes. The first route involves radiationless decay to the ground state, leading to the products of $\text{CH}_2\text{CHCO}(^2A')+\text{H}(^2S)$. The second route involves ISC to the $^3(\pi\pi^*)$ state, followed by dissociation to the ground-state products $\text{CH}_2\text{CH}(^2A')+\text{CHO}(^2A')$. Also, the acrolein molecules in the $^3(\pi\pi^*)$ state can isomerize to $\text{CH}_3\text{CHCO}(^3A'')$, which dissociates easily into $\text{CH}_3\text{CH}(^3A'')+\text{CO}(^1\Sigma^+)$. The resulting $\text{CH}_3\text{CH}(^3A'')$ immediately transforms to the ground-state ethylene. This corresponds to the decarbonylation process, the third photolysis channel of CH_2CHCHO .

Clearly, previous investigations all suggest that nonadiabatic processes, IC and ISC are playing significant roles in the photochemistry of acrolein. The photolysis channels tend to occur in the lower electronic states via IC or ISC processes, though initially excited to a higher state. But there appears to be some conflict regarding the reaction mechanisms derived from previous studies. For example, the decar-

bonylation channel (3) was suggested to proceed in the highly vibrationally excited ground S_0 state following IC^{20,21} but theoretical calculations²⁷ favor a triplet $^3(\pi, \pi^*)$ state mechanism after ISC. For the C—H bond fission channel (2) producing $\text{CH}_2=\text{CHCO}+\text{H}$, theoretical calculations²⁷ predicted a probable mechanism in the ground S_0 state but molecular beam experiments¹⁹ indicated the reactions most likely proceeds in the excited ($^1n\pi^*$) state or ($^3n\pi^*$) state rather than the ground S_0 state.

In this work, we have investigated the photodissociation and photoisomerization dynamics of acrolein ($\text{CH}_2=\text{CHCHO}$) in solution by means of time-resolved Fourier transform infrared (TR-FTIR) absorption spectroscopy. The purpose of performing the photolysis reactions in solution are manifold: (1) extra mechanistic information can be obtained because of two reasons. One is that, the unstable products or intermediates in the gas phase, such as $\text{CH}_2=\text{CHCO}$ and $\text{CH}_3\text{CH}=\text{C}=\text{O}$, can be stabilized in solution and thus captured in the transient infrared absorption spectra. The second is that control experiments monitoring the product yields as a function of triplet quencher concentration can be conveniently performed in solution from which the triplet state reaction mechanism can be elucidated. (2) The solution experiments not only can provide clues clarifying the previous controversial mechanisms but also different photochemistry in solution can be explored by comparing the results with the reported gas phase results. (3) As a prototype molecule, the photochemistry of $\text{CH}_2=\text{CHCHO}$ in solution is of particular interests to various fields utilizing the rich photochemistry of the enone functional group $-\text{C}=\text{C}-\text{C}=\text{O}$ for synthetic methodologies because the realistic photochemical reactions are usually performed in solution rather than gas phase.

II. EXPERIMENTAL AND COMPUTATIONAL METHODS

A. Experiments

The photochemical reactions are monitored by step-scan, TR-FTIR absorption spectroscopy.^{28,29} Step-scan FTIR spectrometers are commercially available but require significant modification for applications on flash photolysis TRIR study. The TR-FTIR absorption instrument (Fig. 1) comprises a Nicolet Nexus 870 step-scan FTIR spectrometer, Lambda Physik (CompexPro102F) Excimer laser, and a pulse generator (Stanford Research DG535) to initiate the laser pulse and achieve synchronization of the laser with data collection, two digitizers (internal 100 KHz 16 bit digitizer and external 100 MHz 14 bit GAGE 14100 digitizer) which offer fast time resolution and a wide dynamic range as needed, and a personal computer to control the whole experiment. The detector used in this work is the photovoltaic MCT-A (0.5 mm) equipped with a fast internal preamplifier (50 MHz).

There are two outputs from the detector: output dc, corresponding to the value of the static interferogram and output ac, corresponding to the time-resolved change of the interferogram. The ac signal was then amplified by an external pre-amplifier (Stanford Research, SRS560). The differential absorbance spectra are calculated based on equation

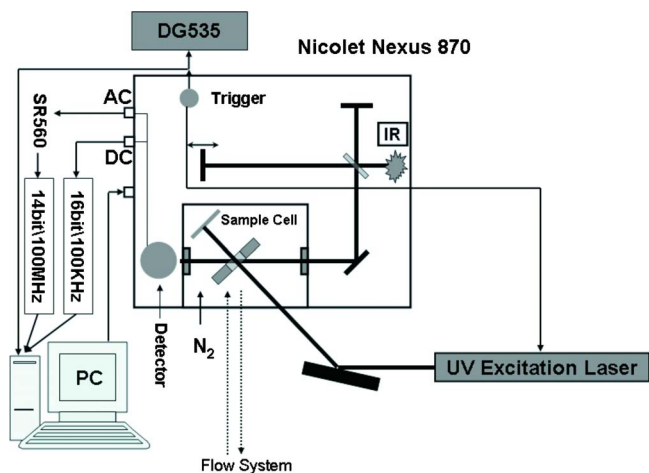


FIG. 1. Schematic experimental setup of the TR-FTIR absorption spectroscopy.

$$\Delta A = A_{ac+dc} - A_{dc} = -\log_{10}(1 + \Delta I_{ac}/I_{dc}),$$

where I_{dc} and ΔI_{ac} are the single-beam intensity spectra corresponding to static (dc) and dynamic (ac) channels. ΔI_{ac} is calibrated before being used in equation because different gain is applied to the ac channel.^{28,29}

ArF excimer laser (193 nm) operating at 10 Hz repetition rate was used in the experiments. The laser excitation beam was directed through an iris aperture (5 mm in diameter) and then overlapped with the infrared beam in the sample cell within the sample compartment of the FTIR spectrometer. The laser beam energy after the aperture was 8 mJ/pulse. A Harrick flowing solution cell with 2-mm-thick CaF₂ windows (path-length: 100 or 500 μ m) was used for the measurements.

CH₂=CHCHO (Alfa, >96%) and *trans*-1, 3-pentadiene (TCI, >97%) were used without further purification. The sample was dissolved in chromatography pure acetonitrile and saturated with Ar (99.999%) before use.

B. Computational methods

Potential energy profiles for the 1,3-H migration reaction pathway of CH₂=CHCHO in both the gas phase and the CH₃CN solution are calculated at the B3LYP/cc-pVDZ level. The polarized continuum model (PCM)³⁰ is used to simulate the effect of the solvent (CH₃CN). The geometries of the reactants, products, intermediates, and transition states along the reaction route in T₁ or S₀ states are optimized using the hybrid density functional theory, i.e., Becke's three-parameter nonlocal exchange functional with the nonlocal correlation functional of Lee, Yang, and Parr (B3LYP) with the cc-pVDZ basis sets.^{31,32} Harmonic vibrational frequencies, relative energies, and the zero-point energies are calculated at the same level with the optimized geometries. The intermediates are characterized by all the real frequencies. The transition states are confirmed by only one imaginary frequency. Connections of the transition states between two local minima have been confirmed by intrinsic reaction coordinate calculations at the same level.³³

To aid spectral assignments, the IR frequencies and IR intensities for all the molecules of interest are calculated at

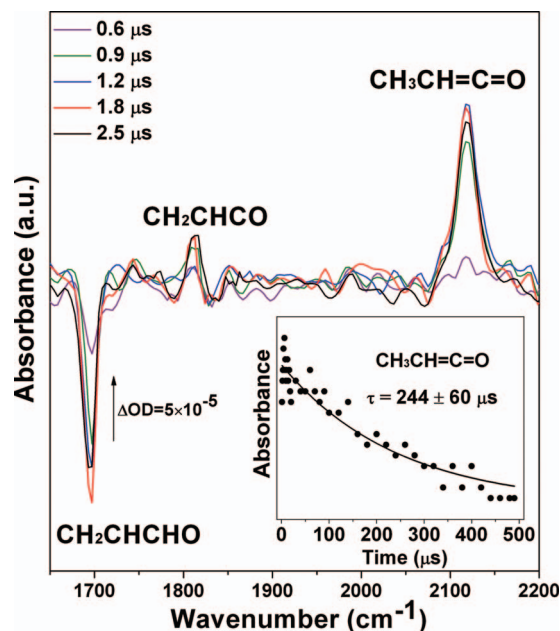


FIG. 2. Infrared transient absorption spectra of 50 mM solution of CH₂=CHCHO in CH₃CN following laser irradiation of 193 nm. Inset: Kinetic traces observed at 2122 cm⁻¹ (CH₃CH=C=O) in CH₃CN solution. The solid line is best fitted with a single-exponential decay function.

the B3LYP/cc-pVDZ level with the solvent (CH₃CN) effect simulated by the PCM model. The harmonic vibrational frequencies are scaled by a factor of 0.96. All of the theoretical calculations are performed with the GAUSSIAN 03 program package.³⁴

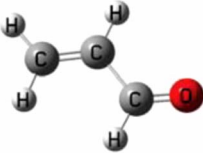
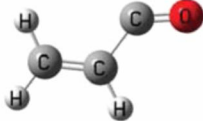
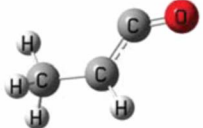
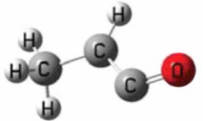
III. RESULTS AND DISCUSSION

A. Identification of photoproducts

Figure 2 displays the time-resolved FTIR absorption spectra in the 0.6–2.5 μ s time interval following the 193 nm irradiation of the 50 mM CH₂=CHCHO solution in acetonitrile. Three transient absorption bands can be clearly identified. The negative band at 1697 cm⁻¹ corresponds to the C=O stretch of the reactant CH₂=CHCHO which undergoes photodepletion, whereas the two positive bands are due to the newly formed photoproducts. The strong band at 2122 cm⁻¹ arises from the 1,3-H migration product, the C=C=O stretch of the methyl ketene CH₃CH=C=O. The weak band at 1807 cm⁻¹ is attributed to the CH₂=CHCO radical from the C–H bond fission reaction.

The above spectral assignments for the three transient infrared absorption bands in Fig. 2 are aided with the quantum chemical calculation. The vibrational frequencies and corresponding infrared intensities are calculated at the B3LYP/cc-pVDZ level and listed in Table I. The PCM is used to simulate the effect of the solvent (CH₃CN). The experimentally observed IR frequency for the stable parent molecule CH₂=CHCHO are measured to be 1697 cm⁻¹ by static FTIR absorption spectra, which is close to the calculated value 1685 cm⁻¹, indicating the current level of calculation can provide accurate and reliable IR frequencies for spectral assignment purpose. As shown in Table I, the calculated IR frequencies 1792 and 2089 cm⁻¹, for the two pho-

TABLE I. IR frequency and IR intensity calculated at the B3LYP/cc-pVDZ level with the solvent (CH_3CN) effect simulated by the PCM model. The harmonic vibrational frequencies are scaled by a factor of 0.96.

Species	Optimized structure	$\nu(\text{C}=\text{O})$ cm^{-1}	IR Intensity (km mol^{-1})
CH_2CHCHO		1685	460
CH_2CHCO		1792	421
$\text{CH}_3\text{CHCO} (\text{T}_1)$		1707	127
$\text{CH}_3\text{CHCO} (\text{S}_0)$		2089	1075

toproducts $\text{CH}_2=\text{CHCO}\cdot$ and $\text{CH}_3\text{CH}=\text{C}=\text{O}$, agrees well with the experimentally observed spectral position of 1807 and 2122 cm^{-1} , respectively. Also, the typical absorption band of carbonyl radical³⁵ and ketene^{36,37} are known to be around 1800 and 2100 cm^{-1} , supporting further these assignments. The 2122 cm^{-1} band observed in the transient infrared absorption spectra arises from the singlet product $\text{CH}_3\text{CH}=\text{C}=\text{O}$ (2089 cm^{-1}), but not the triplet product $\text{CH}_3\text{CH}=\text{C}=\text{O}$ because the latter corresponds to the IR absorption at much lower frequency 1707 cm^{-1} .

The reaction occurs rapidly with both products and reactants reaching simultaneously to their maximum spectral intensity at $1.8\ \mu\text{s}$. At later time, the positive bands of photochemical products are decaying markedly due to some quenching process with different rate. The $\text{CH}_2=\text{CHCO}\cdot$ radical decays within $20\ \mu\text{s}$ with predominantly second-order kinetics resulting from radical-radical recombination, while the stable product $\text{CH}_3\text{CH}=\text{C}=\text{O}$ decays within several hundreds of microseconds with a lifetime of $244 \pm 60\ \mu\text{s}$ as shown in the inset of Fig. 2. The decay kinetics supports further the spectral assignment.

B. Determination of photolysis channels and branching ratios

By identifying the photoproducts from the transient infrared absorption spectra, two photolysis channels of $\text{CH}_2=\text{CHCHO}$ in CH_3CN solution can be elucidated. One is the photoisomerization producing methyl ketene ($\text{CH}_3\text{CH}=\text{C}=\text{O}$) through 1,3-H migration, the other is the photodissociation yielding $\text{CH}_2=\text{CHCO}\cdot$ radical through the C—H bond fission. In previous gas phase studies, both

the experiments^{20,21} and theoretical calculations²⁷ indicated that the CO release channel (3) arises from an isomerization to methyl ketene prior to the dissociation process: $\text{CH}_2=\text{CHCHO} \rightarrow \text{CH}_3\text{CH}=\text{C}=\text{O} \rightarrow \text{CH}_3\text{CH} + \text{CO} \rightarrow \text{CH}_2\text{CH}_2 + \text{CO}$. It is noteworthy that the key intermediate $\text{CH}_3\text{CH}=\text{C}=\text{O}$ leading to the gas phase decarbonylation channel (3) is here directly observed in the solution phase. This result can provide direct evidence supporting the mechanism of the decarbonylation through the prior isomerization to methyl ketene. The reason why the intermediate methyl ketene can be captured in solution is ascribed to the fact that the hot intermediate can be stabilized rapidly by efficient vibrational quenching of solvents, whereas in the gas phase the hot intermediates are subject to facile secondary dissociation into $\text{CH}_2\text{CH}_2 + \text{CO}$ surmounting a very low barrier of 6.5 kcal mol^{-1} .²⁷ Due to the same reason, the photofragments $\text{CH}_2=\text{CHCO}$ yielded from the C—H bond fission channel are also observed in solution, whereas in gas phase the hot fragments undergo secondary dissociation into $\text{CH}_2\text{CH} + \text{CO}$.

To further rationalize the importance of these two photolysis channels, the absolute branching ratios are determined. One advantage of the TR-FTIR absorption spectra is that it measures simultaneously the depletion of parent molecules with the formation of photoproducts. Thus, the amount of the photoproduct formation and parent consumption can both be quantified by normalizing the peak area of the IR absorption band with the absorption coefficient. While experimentally hard to determine especially for transient species, the IR absorption coefficients can be acquired by *ab initio* calculations with the GAUSSIAN program which gives the IR intensity while computing the IR frequency of a spe-

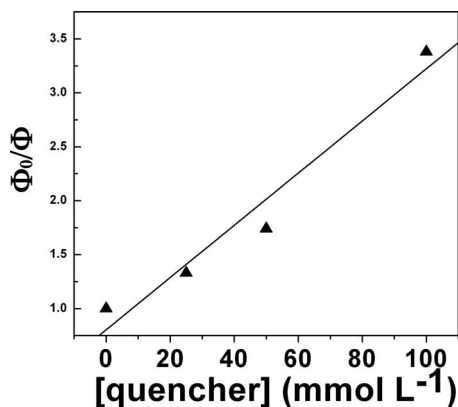


FIG. 3. Stern–Volmer plot of the photoproduct (CH₃CH=C=O) yield varied with the addition of the triplet quencher, *trans*-1,3-pentadiene.

cific vibrational mode, as shown in Table I. The computed IR intensity in the unit of km mol⁻¹ actually denotes the integrated IR absorption coefficient.³⁸ The calculations are believed to predict relative IR intensities in excellent agreement with experiment.³⁸

Dividing the amount of photoproduct formation by the parent consumption gives the absolute branching ratios which is 0.12 and 0.78 for the two photoproducts of CH₂=CHCO and CH₃CH=C=O, respectively. The sum of these two ratios is close to 1.0, suggesting that the α cleavage of C–H bond and the 1,3-H migration account for most of the photochemical reactions of CH₂CHCOH in solution. Relative to the total photochemical reaction, the 1,3-H migration is shown to be the predominant channel, accounting for the largest fraction yield in solution.

C. Photodissociation and photoisomerization Mechanisms

For the 1,3-H migration channel, it has been suggested by the gas phase experiments^{20,21} that the reaction is likely to proceed in the highly vibrationally excited ground S₀ state following IC but theoretical calculations²⁷ favor a triplet ³($\pi\pi^*$) state mechanism via ISC. The question arises whether the photoisomerization is associated to the S₀ state or triplet ³($\pi\pi^*$) state. Here in solution we perform control experiments to monitor the yield of the isomerization product CH₃CH=C=O varied with the addition of the triplet quencher *trans*-1,3-pentadiene. Assuming the reaction occurs through the triplet ³($\pi\pi^*$) state, the quencher addition is expected to lower the yield of CH₃CH=C=O. Indeed, the product yield decreased as the concentration of quencher increased. It is generally assumed that if only one excited state is involved in a photochemical reaction, a Stern–Volmer plot of ϕ_0/ϕ (where ϕ_0 is the quantum yield of the reaction and ϕ is the quantum yield in the presence of quencher, both can be determined from TR-FTIR spectra) versus the quencher concentration shows a straight line.³⁹ Actually, an excellent linear correlation ($R^2=0.96$) is obtained with the Stern–Volmer plot for the product yield varied with the triplet quencher, as shown in Fig. 3. This result clearly suggests that, most (if not all) of the photoisomerization reaction of

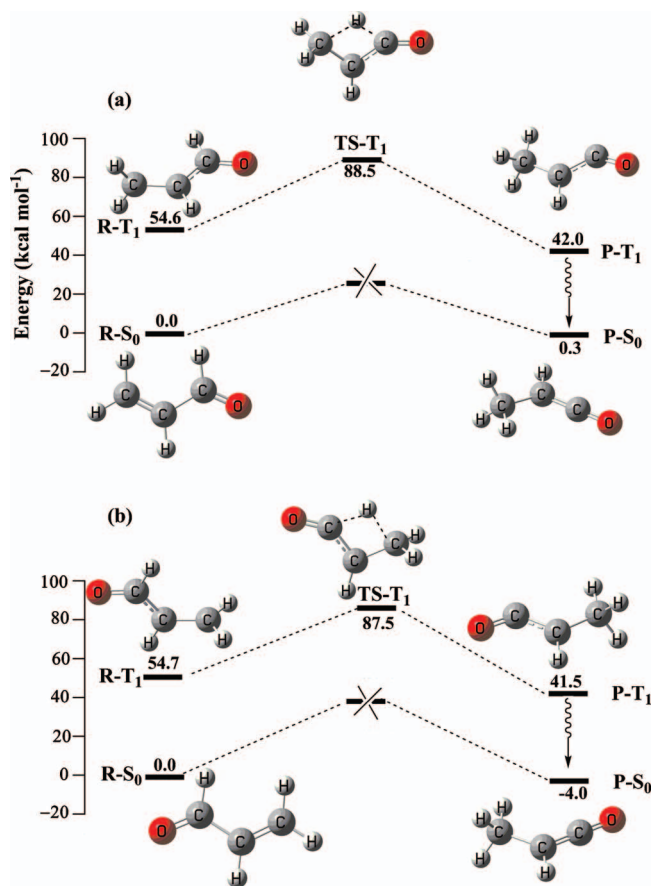
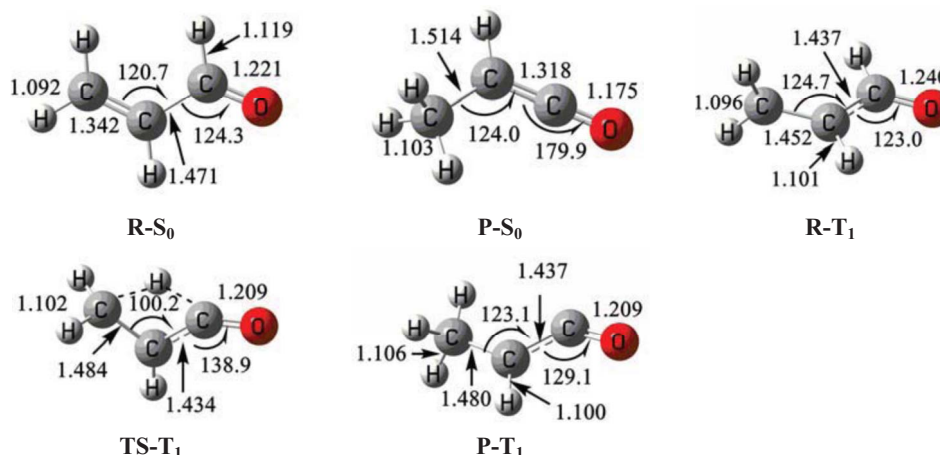


FIG. 4. Energy profiles along an arbitrary reaction coordinate showing the 1,3-H migration reaction pathway of CH₂=CHCHO in the (a) CH₃CN solution and (b) gas phase. Relative energy values obtained from the ZPVE-corrected B3LYP/cc-pvdz total energies. The PCM is used to simulate the effect of the solvent (CH₃CN).

1,3-H migration is correlated to the triplet ³($\pi\pi^*$) state rather than the ground S₀ state.

Why does the photoisomerization take place in the triplet ³($\pi\pi^*$) state instead of the ground S₀ state? According to the theoretical calculations,²⁷ the S₀/S₁¹($n\pi^*$) conical intersection point occurs at a perpendicular structure with the terminal CH₂ group twisted 90° and lies about 15 kcal mol⁻¹ in energy above the ¹($n\pi^*$) minimum. In contrast, the ¹($n\pi^*$)/³($\pi\pi^*$) crossing point occurs at a planar geometry which is structurally close to the ¹($n\pi^*$) minimum. This crossing point is only 4 kcal mol⁻¹ above the energy of the ¹($n\pi^*$) minimum. Therefore, it can be expected that the ISC to the ³($\pi\pi^*$) state takes place much more easily than does the IC to the ground state via the S₀/S₁ crossing point. After photoexcitation at 193 nm, acrolein relaxes to the ¹($n\pi^*$) state. From this state, the system decays to the ³($\pi\pi^*$) state through the ¹($n\pi^*$)/³($\pi\pi^*$) crossing point, followed by isomerization to CH₃CH=C=O through 1,3-H migration in the ³($\pi\pi^*$) state. On the other hand, even though some fraction of molecules undergo S₁→S₀ IC, the 1,3-H migration does not occur in the ground S₀ state according to the following theoretical calculations.

Figure 4 shows the potential energy profiles we have calculated at the B3LYP/cc-pVDZ level for the 1,3-H migration of CH₂=CHCHO in both the gas phase and the CH₃CN

TABLE II. Optimized geometries of reactants, intermediates, transition states, and products for the 1,3-H migration of $\text{CH}_2=\text{CHCOH}$ in CH_3CN solution at the level of B3LYP/cc-pVDZ. Bond lengths are in angstrom.

solution. The optimized stationary structures along the reaction pathways are listed in Table II. Similar potential energy profiles and stationary structures are obtained for the gas phase and solution phase reactions. As shown in Fig. 4, no transition states can be located linking the reactant with the isomerization product in the S_0 state indicating that the 1,3-H migration can not proceed in the ground S_0 state. Instead, the 1,3-H migration reaction is feasible in the triplet state through a four-membered cyclic transition state, surmounting a reaction barrier of $33.9 \text{ kcal mol}^{-1}$ (in solution) or $32.8 \text{ kcal mol}^{-1}$ (in the gas phase). It is interesting to note here that the 1,3-H migration reaction becomes a facile process in the T_1 state although totally infeasible in the S_0 state. As shown in Table II, the ethylenic bond of the T_1 state of $\text{CH}_2=\text{CHCHO}$ actually becomes a single bond because the T_1 state originates from the $\text{C}=\text{C}\pi \rightarrow \pi^*$ excitation. Thus, the T_1 state $\text{CH}_2=\text{CHCHO}$ behaves like a biradical with the two carbon atoms being partitioned with unpaired electrons which could provide extra driving force facilitating the 1,3-H migration in the T_1 state.

For the photodissociation channel (2) producing $\text{CH}_2=\text{CHCO}+\text{H}$, the past investigations have proposed several different mechanisms. The CASSCF calculations²⁷ showed that the ground-state products $\text{CH}_2=\text{CHCO}$ (${}^2A'$) + $\text{H}({}^2S)$ correlate adiabatically with the ground-state and the ${}^3(\pi\pi^*)$ state of acrolein, but there is a large barrier in the ${}^3(\pi\pi^*)$ state. In the ground electronic state, there is no barrier to C—H bond fission above the endothermicity ($83.2 \text{ kcal mol}^{-1}$ at the CAS(8,7)/cc-pVDZ level of theory with zero-point correction). Therefore, the most probable mechanism of the C—H bond fission was proposed to take place after IC to the ground state. Meanwhile, the CASSCF calculations²⁷ also showed that a second set of products $14.9 \text{ kcal mol}^{-1}$ above the ground-state products, $\text{CH}_2=\text{CHCO}$ (${}^2A''$) + $\text{H}({}^2S)$, correlates adiabatically with the excited ${}^1(n\pi^*)$ state and the ${}^3(n\pi^*)$ state. Both states have a small barrier to the reverse reaction, $\sim 2.1 \text{ kcal mol}^{-1}$ for the ${}^1(n\pi^*)$ state and $0.7 \text{ kcal mol}^{-1}$ for the ${}^3(n\pi^*)$ state. Such a type of C—H bond fission yielding the excited state prod-

ucts $\text{CH}_2=\text{CHCO}$ (${}^2A''$) + $\text{H}({}^2S)$ was later probed by the H-atom Rydberg tagging experiment of Butler *et al.*¹⁹ This work suggested that the C—H bond fission channel probably proceeds in the excited ${}^1(n\pi^*)$ state or ${}^3(\pi\pi^*)$ state rather than the ground S_0 state since the dissociation in the excited states involves a certain barrier in the exit channel, consistent with the observation of a translational energy distribution peaked away from 0.

Here in solution phase photolysis experiments, which is the mechanism accounting for the C—H bond fission channel? When performing the control experiments of triplet quencher, we also observed that the yield of the C—H bond fission product $\text{CH}_2=\text{CHCO}\cdot$ did not vary with the addition of the triplet quencher, indicating that the photodissociation channel is not associated to either the triplet ${}^3(n\pi^*)$ or ${}^3(\pi\pi^*)$ state, but rather a singlet state. Two singlet states S_1 and S_0 could be possibly involved. According to the CASSCF calculations,²⁷ the S_1 ${}^1(n\pi^*)$ state correlates with the excited products $\text{CH}_2=\text{CHCO}$ (${}^2A''$) + $\text{H}({}^2S)$ and requires surmounting a barrier of $28.9 \text{ kcal mol}^{-1}$. In the ground S_0 state there is no barrier above the endothermicity of $83.2 \text{ kcal mol}^{-1}$ and the ground-state products $\text{CH}_2=\text{CHCO}$ (${}^2A'$) + $\text{H}({}^2S)$ are formed.²⁷ The S_0/S_1 conical intersection lies about 15 kcal mol^{-1} higher than the S_1 minimum.²⁷ Energetically, it appears that the IC to the S_0 state via the S_0/S_1 conical intersection is more efficient than the C—H bond fission in the S_1 state which has a barrier of $28.9 \text{ kcal mol}^{-1}$. The C—H bond fission might occur in the S_0 state as a result of the S_1 - S_0 IC. However, the $S_1 \rightarrow S_0$ IC is expected to be unfavorable because the S_0/S_1 conical intersection point occurs at a perpendicular geometry with the terminal CH_2 group twisted 90° which is structurally different from the S_1 minimum.²⁷ In addition, the ultrafast solvent vibrational quenching can dissipate the excitation energy rapidly and thus suppress the dissociation reaction in solution. In this case, the direct dissociation in the S_1 ${}^1(n\pi^*)$ state should be less suppressed than the indirect dissociation (after the S_1 - S_0 IC) in the S_0 state which requires normally longer

time to transfer at least 83.2 kcal mol⁻¹ to the C—H bond in order for a hydrogen atom to dissociate. Dissociation from the hot ground electronic state is expected to be significantly prohibited due to the solvent quenching effect. In solution, it is more likely that the C—H bond fission proceeds in the S₁¹(nπ*) state although the contribution of the S₀ pathway could not be totally ruled out. Given the fact that the gas phase H-atom Rydberg tagging experiment of Butler *et al.*¹⁹ also suggested that the excited S₁¹(nπ*) state rather than the ground S₀ state consisted with the observation of a translational energy distribution peaked away from 0, the most probable scenario in solution could be deduced that the excited molecules undergo C—H bond fission in the S₁¹(nπ*) state yielding the product CH₂=CHCO (²A'') + H(²S), and the excited state products decay to their ground-state CH₂=CHCO (²A'') + H(²S) eventually. As shown in the transient infrared absorption spectra (Fig. 2.), the ground-state radical CH₂=CHCO (²A') is observed.

D. Comparison with the gas phase results

Overall, it shows here that in solution the acrolein (CH₂CHCHO) molecules upon 193 nm excitation undergo two photochemical reactions. One is the 1,3-H migration accounting for the largest yield (0.78) and the other is the α cleavage of the C—H bond with a yield of only 0.12. Another possible channel of the C—C bond cleavage forming HCO + CH₂=CH is not observed in solution. Assuming this channel is undetectable in solution due to some unknown reasons, the yield of this channel can still be estimated to be less than 0.10 since the sum of the other observed channels already account for 0.90 yields.

NO measurements were reported of product branching ratios in the gas phase photolysis investigations. Only some qualitative estimation mentioned the relative importance of different channels. The C—C bond cleavage forming HCO + CH₂=CH was suggested to be the most important channel in the gas phase based on the theoretical calculations,²⁷ which is in agreement with the experimental observation of CH₂CH and HCO as the only primary products for the photofragmentation of acrolein in supersonic molecular beam at 193 nm.²²

Evidently, from gas phase to solution, the relative importance of photolysis channels varies a lot. The photochemistry in solution turns out to be quite different from the gas phase. In solution, the photoisomerization of 1,3-H migration is the predominant channel and the photoinduced bond cleavage reactions appears to account for much less yield, while the photodissociation of bond cleavage seems to be dominant in the gas phase. Most likely, the solvent interaction plays significant roles leading to the different photochemistry in solution. For example, the radical photofragments, HCO + CH₂=CH or CH₂=CHCO + H, can easily recombine in the solvent cage forming back to their precursor molecules, and thus the branching ratios of photodissociation channels are significantly reduced in solution. On the other hand, the photoisomerization forming stable rearrangement products CH₃CH=C=O are not subject to recombination and thus tends not to be affected by the solvent. While the photodis-

sociation channels are greatly prohibited in solution, the photoisomerization takes over and becomes dominant.

IV. CONCLUSION

For the prototype molecule of α,β-enones, acrolein (CH₂=CHCHO), we have investigated its 193 nm photodissociation and photoisomerization dynamics in solution. By means of TR-FTIR absorption spectroscopy, the primary photolysis channels and absolute branching ratios are determined. The predominant channel is shown to be the 1,3-H migration yielding the rearrangement product CH₃CH=C=O with a branching ratio of 0.78 and the less important channel is the α cleavage of C—H bond yielding radical fragments CH₂=CHCO + H with a branching ratio of only 0.12. Moreover, the most probable reaction mechanisms are clarified by control experiments monitoring the product yields varied with the triplet quencher addition. The 1,3-H migration is strongly suggested to correlate with the triplet ³(ππ*) state rather than the ground S₀ state by the experimental evidence which shows that the product yield decreases with the addition of triplet quencher and the Stern–Volmer plot of φ₀/φ versus the quencher concentration exhibits an excellent linear correlation. On the other hand, the α cleavage of C—H bond is shown not to be associated with triplet states, but is more likely to proceed in the S₁¹(nπ*) state in solution.

Compared to the gas phase photolysis which is dominated by photodissociation channels, the most important channel in solution is the photoisomerization of 1,3-H migration. The reason leading to the different photochemistry in solution can be ascribed to the solvent cage effect. The distinct solution phase photochemistry of acrolein revealed here is of great importance to understand the reaction mechanisms of this type of α,β-enones molecules in general and the photochemistry affected by solvent interaction.

ACKNOWLEDGMENTS

This work is financially supported by the National Natural Science Foundation of China (Grant Nos. 20733005, 20673126, and 20973179), the National Basic Research Program of China (Grant Nos. 2007CB815200 and 2007AA02Z116), and the Chinese Academy of Sciences.

¹D. I. Schuster, G. Lem, and N. A. Kaprinidis, *Chem. Rev. (Washington, D.C.)* **93**, 3 (1993).

²A. G. Griesbeck, N. Hoffmann, and K. Warzecha, *Acc. Chem. Res.* **40**, 128 (2007).

³N. Hoffmann, *Chem. Rev. (Washington, D.C.)* **108**, 1052 (2008).

⁴I. Gómez, S. Olivella, M. Reguero, A. Riera, and A. Solé, *J. Am. Chem. Soc.* **124**, 15375 (2002).

⁵H. E. Zimmerman and E. E. Nesterov, *J. Am. Chem. Soc.* **125**, 5422 (2003).

⁶J. Blanco-Urgoiti, L. Anorbe, S. L. Perez, G. Dominguez, and C. Perez, *Chem. Soc. Rev.* **33**, 32 (2004).

⁷S. E. Gibson and A. Stevenazzi, *Angew. Chem., Int. Ed.* **42**, 1800 (2003).

⁸E. Paterno and G. Chieffi, *Gazz. Chim. Ital.* **39**, 341 (1909).

⁹G. Büchi, C. G. Inman, and E. S. Lipinsky, *J. Am. Chem. Soc.* **76**, 4327 (1954).

¹⁰J. Singh, *Photochemistry and Pericyclic Reactions* (New Age International, New Delhi, India, 2005).

¹¹C. W. Spangler, *Chem. Rev. (Washington, D.C.)* **76**, 187 (1976).

¹²A. C. P. Alves, J. Christoffersen, and J. M. Hollas, *Mol. Phys.* **20**, 625

- (1971).
- ¹³ A. D. Walsh, *Trans. Faraday Soc.* **41**, 498 (1945).
- ¹⁴ R. S. Becker, K. Inuzuka, and J. King, *J. Chem. Phys.* **52**, 5164 (1970).
- ¹⁵ C. E. Dykstra, *J. Am. Chem. Soc.* **98**, 7182 (1976).
- ¹⁶ E. R. Davidson and L. E. Nitzsche, *J. Am. Chem. Soc.* **101**, 6524 (1979).
- ¹⁷ K. Valenta and F. Grein, *Can. J. Chem.* **60**, 601 (1982).
- ¹⁸ H. Shinohara and N. Nishi, *J. Chem. Phys.* **77**, 234 (1982).
- ¹⁹ B. F. Parsons, D. E. Szpunar, and L. J. Butler, *J. Chem. Phys.* **117**, 7889 (2002).
- ²⁰ M. E. Umstead, R. G. Shortridge, and M. C. Lin, *J. Phys. Chem.* **82**, 1455 (1978).
- ²¹ G. T. Fujimoto, M. E. Umstead, and M. C. Lin, *J. Chem. Phys.* **82**, 3042 (1985).
- ²² B. M. Haas, T. K. Minton, P. Felder, and J. R. Huber, *J. Phys. Chem.* **95**, 5149 (1991).
- ²³ A. Devaquet and L. Salem, *Can. J. Chem.* **49**, 977 (1971).
- ²⁴ A. Devaquet, *J. Am. Chem. Soc.* **94**, 5160 (1972).
- ²⁵ R. R. Lucchese, H. F. Schaefer, and C. E. Dykstra, *Chem. Phys. Lett.* **51**, 600 (1977).
- ²⁶ M. Reguero, M. Olivucci, F. Bernardi, and M. A. Robb, *J. Am. Chem. Soc.* **116**, 2103 (1994).
- ²⁷ W. H. Fang, *J. Am. Chem. Soc.* **121**, 8376 (1999).
- ²⁸ W. Uhmann, A. Becker, C. Taran, and F. Siebert, *Appl. Spectrosc.* **45**, 390 (1991).
- ²⁹ D. L. Drapcho, P. Curbelo, E. Y. Jiang, R. A. Crocombe, and W. J. McCarthy, *Appl. Spectrosc.* **54**, 453 (1997).
- ³⁰ M. Cossi, V. Barone, and M. A. Robb, *J. Chem. Phys.* **111**, 5295 (1999).
- ³¹ A. D. Becke, *J. Chem. Phys.* **98**, 5648 (1993).
- ³² C. Lee, W. Yang, and R. G. Parr, *Phys. Rev. B* **37**, 785 (1988).
- ³³ C. Gonzalez and H. B. Schlegel, *J. Phys. Chem.* **94**, 5523 (1990).
- ³⁴ M. J. Frisch, G. W. Trucks, H. B. Schlegel *et al.*, GAUSSIAN 03, Revision B.03, Gaussian, Inc., Pittsburgh, PA, 2003.
- ³⁵ A. G. Neville, C. E. Brown, D. M. Rayner, J. Luszyk, and K. U. Ingold, *J. Am. Chem. Soc.* **113**, 1869 (1991).
- ³⁶ V. D. Lin, N. B. Cothup, W. G. Fateley, and J. G. Graselli, *The Handbook of Infrared and Raman Characteristic Frequencies of Organic Molecules* (Academic, San Diego, 1991).
- ³⁷ T. T. Tidwell, *Ketenes* (Wiley, New York, 1995).
- ³⁸ B. A. Hess and L. J. Schaad, *Chem. Rev. (Washington, D.C.)* **86**, 709 (1986).
- ³⁹ N. J. Turro, *Modern Molecular Photochemistry* (University Science Books, Sausalito, CA, 1991).